MOLECULAR AND CELLULAR BIOLOGY, July 2005, p. 6722–6733 Vol. 25, No. 15
0270-7306/05/$08.00+0 doi:10.1128/MCB.25.15.6722–6733.2005

Individual Palmitoyl Residues Serve Distinct Roles in H-Ras Trafficking, Microlocalization, and Signaling

Sandrine Roy,[1] Sarah Plowman,[1] Barak Rotblat,[2] Ian A. Prior,[3] Cornelia Muncke,[1] Sarah Grainger,[1] Robert G. Parton,[1,4] Yoav I. Henis,[2] Yoel Kloog,[2] and John F. Hancock[1]*

Institute for Molecular Bioscience[1] and Centre for Microscopy and Microanalysis,[4] University of Queensland, Brisbane, Australia; Department of Neurobiochemistry, George S. Wise Faculty of Life Sciences, Tel Aviv University, Tel Aviv, Israel[2]; and The Physiological Laboratory, Crown Street, University of Liverpool, Liverpool, England[3]

Received 28 February 2005/Returned for modification 3 April 2005/Accepted 9 May 2005

H-ras is anchored to the plasma membrane by two palmitoylated cysteine residues, Cys181 and Cys184, operating in concert with a C-terminal *S*-farnesyl cysteine carboxymethylester. Here we demonstrate that the two palmitates serve distinct biological roles. Monopalmitoylation of Cys181 is required and sufficient for efficient trafficking of H-ras to the plasma membrane, whereas monopalmitoylation of Cys184 does not permit efficient trafficking beyond the Golgi apparatus. However, once at the plasma membrane, monopalmitoylation of Cys184 supports correct GTP-regulated lateral segregation of H-ras between cholesterol-dependent and cholesterol-independent microdomains. In contrast, monopalmitoylation of Cys181 dramatically reverses H-ras lateral segregation, driving GTP-loaded H-ras into cholesterol-dependent microdomains. Intriguingly, the Cys181 monopalmitoylated H-ras anchor emulates the GTP-regulated microdomain interactions of N-ras. These results identify N-ras as the Ras isoform that normally signals from lipid rafts but also reveal that spacing between palmitate and prenyl groups influences anchor interactions with the lipid bilayer. This concept is further supported by the different plasma membrane affinities of the monopalmitoylated anchors: Cys181-palmitate is equivalent to the dually palmitoylated wild-type anchor, whereas Cys184-palmitate is weaker. Thus, membrane affinity of a palmitoylated anchor is a function both of the hydrophobicity of the lipid moieties and their spatial organization. Finally we show that the plasma membrane affinity of monopalmitoylated anchors is absolutely dependent on cholesterol, identifying a new role for cholesterol in promoting interactions with the raft and nonraft plasma membrane.

Ras GTPases operate as plasma membrane-localized molecular switches that regulate multiple signal transduction pathways. The three ubiquitously expressed Ras isoforms, H-, N-, and K-ras, are anchored to the inner surface of the plasma membrane by a C-terminal *S*-farnesyl cysteine carboxy methylester acting in concert with a second signal. The *S*-farnesyl cysteine carboxy methylester is generated by a triplet of post-translational modifications of the C-terminal CAAX motif that is common to all Ras proteins. The second signal in K-ras comprises a polybasic domain of 6 lysine residues (17–19, 21). In contrast, the second signal in H- and N-ras comprises palmitoylation of cysteine residues. In N-ras a single cysteine (Cys181) is palmitoylated, but in H-ras two cysteines (Cys181 and Cys184) are palmitoylated (19, 21).

A two-signal membrane-targeting mechanism is common in biological systems (44) and in the case of Ras proteins serves to determine the trafficking pathway taken to the plasma membrane and the microlocalization of each isoform within the plasma membrane. For example, H-ras traffics through the exocytic pathway to the plasma membrane, where it exists in a GTP-regulated equilibrium between cholesterol-dependent lipid rafts and nonraft microdomains. K-ras reaches the plasma membrane from the endoplasmic reticulum (ER) via an undefined pathway and localizes to nonraft microdomains that are spatially distinct from those occupied by activated H-ras (35, 41, 43, 50). H-ras and K-ras generate distinct signal outputs from their different plasma membrane microdomains (16, 20). The microlocalization of N-ras on the plasma membrane has not to date been extensively studied (20). In addition to signaling from the plasma membrane, H-ras and N-ras are also able to generate signals from internal membranes such as the Golgi apparatus (5–7, 38) and endosomes (27, 46, 51) that are quantitatively distinct from those generated at the plasma membrane. In combination the different signal outputs from the multiple platforms on which H-ras, N-ras, and K-ras operate can readily account for the marked biological differences between these Ras proteins (16).

A critical enzyme for H- and N-ras function is Ras palmitoyltransferase (PAT) (30). Ras PAT is localized predominantly to the ER in yeast and to the ER and Golgi apparatus in mammalian cells (1, 7, 30, 57). PATs have also been characterized with non-Ras substrates, although it remains unclear to what extent this class of enzymes exhibits true substrate fidelity (14, 23, 29, 33). There is evidence that some proteins may be acylated directly at the plasma membrane (11, 54), including perhaps N-ras (52). Acyltransferase activity towards $G\alpha_i$ has been detected in biochemical preparations of lipid rafts (11).

Palmitoylation, in contrast to farnesylation, is reversible.

* Corresponding author. Mailing address: Institute for Molecular Bioscience, 306 Carmody Road, University of Queensland, Brisbane 4072, Australia. Phone: 61-7-3346-2033. Fax: 61-7-3346-2101. E-mail: j.hancock@imb.uq.edu.au.

Several factors contribute to the overall half-life of palmitate on palmitoylated proteins, including the number of acyl linkages, the activation state of the protein, and general accessibility to PATs and thioesterases. Although lysosomal thioesterases have been identified (55), a selective Ras thioesterase that removes palmitate from Ras has yet to be identified. Biochemical studies suggest, however, that access to esterases and not sequence recognition may be important for palmitate turnover (31). The half-life of palmitate on N-ras is 20 min and for H-ras it is 2.4 h, in contrast to a half-life of 24 h for the protein backbone (3, 31, 32). It is possible that the double palmitoylation of H-ras compared to N-ras is responsible for this longer half-life of palmitate. Interestingly, the turnover of palmitate on GTP-loaded H-ras is 2.4 times faster than on GDP-loaded H-ras (3). An important consequence of palmitate turnover is that the membrane anchor of H- and N-ras is constantly being destroyed and resynthesized. This would be expected to have profound effects on plasma membrane tethering and trafficking, or recycling, of the proteins between the ER and Golgi apparatus and plasma membrane. Palmitate turnover could therefore regulate H- and N-ras function, albeit on a different time scale (minutes) than changes in microlocalization (milliseconds).

Microlocalization of Ras proteins at the plasma membrane is determined by interactions between the C-terminal membrane anchor and the lipid bilayer together with scaffold proteins such as Sur-8 and galectin-1 all operating within the confines of a submembrane actin fence (20). In the case of H-ras these interactions are further modulated by the guanine nucleotide-bound state of the protein. We have shown recently that the minimal membrane anchor of H-ras efficiently targets to lipid rafts and that the adjacent hypervariable region provides affinity, perhaps through the binding of galectin-1, to nonraft microdomains (48). The G domain repels H-ras from the membrane, lowering its affinity for rafts and allowing the interaction with, or generation of, nonraft microdomains. The repulsive force is greater when H-ras is GTP loaded, offering a basic mechanism for how the lateral segregation of H-ras may be regulated (48). Ultimately this model will need to be refined with data on precisely how the C-terminal anchor of H-ras inserts into lipid bilayers and how GTP loading modulates this insertion. Recent studies investigating the structure and interaction of an N-ras C-terminal membrane anchor with model membranes are beginning to define the biophysical principles underlying the membrane attachment of prenylated and palmitoylated anchors (15, 24, 26). These studies show how the single palmitate of N-ras operating with the C-terminal prenylated, methylated cysteine inserts the C-terminal peptide sequence deep within the membrane bilayer. No such study has been reported for H-ras, and it is difficult to predict how an additional palmitate on Cys184 would modify membrane anchoring. It is also unknown whether a single palmitate would be sufficient to allow normal regulation of H-ras lateral segregation.

In this report we examine how the function of H-ras is influenced by double palmitoylation and whether specific functions can be attributed to the individual palmitates on Cys181 and Cys184. We examine to what extent monopalmitoylated H-ras operates like N-ras by investigating activation of downstream effectors, subcellular localization, trafficking, and plasma membrane microlocalization.

MATERIALS AND METHODS

Plasmids. Green fluorescent protein (GFP)–H-rasG12V and GFP–H-ras expression vectors have been described previously (1, 19, 41). GFP–H-ras C181S and C184S (wild type and G12V) were subcloned into EGFP-C1 (Clontech) from plasmids described previously (19).

Antibodies and reagents. Affinity-purified polyclonal antibody against monomeric red fluorescent protein (mRFP) was generated as described previously for affinity-purified polyclonal antibody against GFP (42, 43). Raf-1 antibody was purchased from Transduction Laboratories. Monoclonal GFP antibody was purchased from Roche. Phospho-mitogen-activated protein kinase and Ras antibodies were purchased from Cell Signaling. Erk antibody was purchased from Santa Cruz. Gold-conjugated antibodies were prepared by the tannic acid-citrate method (43). Gold antibody conjugates (2- and 4-nm particle size) were purified on 10 to 40% glycerol gradients (43).

Cell transfection and immunofluorescence. Baby hamster kidney (BHK) cells were grown and maintained in HEPES-buffered Dulbecco's modified Eagle's medium containing 10% donor calf serum, as described previously (50). BHK cells were seeded onto either coverslips for immunofluorescence or 10-cm dishes for biochemical assays and transfected using Lipofectamine (Life Technologies) according to the manufacturer's instructions. The efficiency of transfection was typically 65 to 80%. Cells on coverslips were fixed 24 h after lipofection and processed for direct fluorescence microscopy. Where indicated, transfected cells were incubated in 50 μg/ml cycloheximide for 5 h or cycloheximide for 2 h followed by 50 μM 2-bromopalmitate (2-BP) plus cycloheximide for a further 3 h before fixation. Cells on 10-cm dishes were switched to serum-free medium 18 to 24 h after lipofection and incubated for a further 4 h before being harvested.

PC12 cells were cultured in Dulbecco's modified Eagle's medium supplemented with 5% horse serum, 10% calf serum, and 2 mM L-glutamine and transfected on coverslips using Lipofectamine. Sixteen hours after lipofection, the cells were returned to standard PC12 culture medium and incubated for a further 48 h prior to processing for confocal microscopy.

Confocal microscopy. Transfected PC12 or BHK cells were washed with phosphate-buffered saline (PBS) and fixed with 4% paraformaldehyde for 30 min at room temperature. Coverslips were mounted in Mowiol for confocal microscopy (1).

Electron microscopy and statistical analysis. BHK cells were transfected with Lipofectamine according to the manufacturer's instructions. Where indicated, cells were treated with 1% methyl-β-cyclodextrin (MβCD) in serum-free medium for 30 min prior to processing. Plasma membrane sheets were prepared, fixed with 4% paraformaldehyde–0.1% glutaraldehyde, and labeled with affinity-purified anti-GFP antisera coupled directly to 4 nm gold as described previously (36, 42, 43). Digital images of the immunogold-labeled plasma membrane sheets were taken at 100,000× magnification in an electron microscope. Intact 1-μm^2 areas of the plasma membrane sheet were identified using Image J, and the x and y coordinates of the gold particles were determined as described previously (42, 43). Ripley's K-function (4, 45) was calculated according to equations 1 and 2 using the x and y coordinates and then standardized on the 99% confidence interval (CI) estimated from equation 3 (43). Bootstrap tests to examine differences between replicated point patterns were constructed exactly as described previously (10), and statistical significance was evaluated against 1,000 bootstrap samples.

$$K(r) = A\, n^{-2} \sum_{j \neq i} w_{ij}\, 1\,(\|x_i - x_j\| \leq r) \quad (1)$$

$$L(r) - r = \sqrt{K(r)/\pi} - r \quad (2)$$

$$\mathrm{CI} = \pm 1.68\, n^{-1} \sqrt{A} \quad (3)$$

$K(r)$ is the K-function for a pattern of n points in an area A, $\|x_i - x_j\|$ is Euclidean distance, $1(\|x_i - x_j\| \leq r)$ is the indicator function, w_{ij}^{-1} is the proportion of the circumference of the circle with center x_i and radius $\|x_i - x_j\|$ contained within A, and r is the radius at which $K(r)$ is calculated.

Fluorescence recovery after photobleaching (FRAP). COS-7 cells were maintained as described previously (12). For FRAP studies, they were plated on glass coverslips in 35-mm-diameter dishes and transfected using DEAE-dextran. At 24 h posttransfection, some samples were cholesterol depleted by a 24-h incubation with 50 μM compactin and 50 μM mevalonate in Dulbecco's modified Eagle's medium containing 10% lipoprotein-deficient serum (22, 35). This pro-

cedure reduces membrane cholesterol content by 30 to 33% (35, 53) and was used because MβCD treatment has been reported to reduce the lateral diffusion rates of some nonraft proteins (35, 53). FRAP studies were conducted 48 h posttransfection at 22°C in Hanks' balanced salt solution supplemented with 20 mM HEPES, pH 7.2, as described previously (35). The monitoring argon ion laser beam (488 nm, 1.2 μW) was focused through a Zeiss Universal microscope to a Gaussian radius of 0.85 ± 0.02 μm (63× objective) or 1.36 ± 0.04 μm (40× objective). A brief pulse (6 mW for 4 to 6 ms for the 63× objective and 10 to 20 ms for the 40× objective) bleached 50 to 70% of the fluorescence in the illuminated region, with recovery monitored by the attenuated monitoring beam. The apparent characteristic fluorescence recovery time, τ (the time required to attain half of the recoverable fluorescence intensity for a Gaussian bleach profile), and the mobile fraction were derived by nonlinear regression analysis, fitting to a lateral diffusion process with a single τ value (39). Statistical comparisons were carried out using Student's *t* test.

Western blotting. Cells were washed and subjected to hypotonic lysis, and P100 and S100 fractions were prepared from postnuclear supernatants as described previously (19). A total of 20 μg of each P100 fraction and an equal proportion of the S100 fraction were immunoblotted for GFP, mRFP, or Raf-1. Blots developed using enhanced chemiluminescence were visualized and quantified by phosphorimaging (49).

Raf-1 kinase assays. P100 aliquots of transfected BHK cells were normalized for protein content and assayed for Raf activity by using a two-stage coupled MEK/ERK assay with phosphorylation of myelin basic protein used as a readout, as described previously (49).

[^{3}H]palmitic acid labeling. BHK cells transiently expressing Ras proteins were treated with 50 μM/ml cycloheximide for 3 h and then labeled with 0.5 mCi of [^{3}H]palmitic acid for a further 2 h in the continued presence of cycloheximide. Cells were harvested in lysis buffer (50 mM Tris, pH 7.5, 75 mM sodium chloride, 25 mM sodium fluoride, 5 mM magnesium chloride, 5 mM EGTA, 1% NP-40, leupeptin, and aprotinin), and 400 μg of whole-cell lysate was immunoprecipitated using monoclonal GFP antibody coupled to protein G-agarose. Immunoprecipitated GFP-ras proteins were washed and eluted in low-dithiothreitol Laemmli sample buffer. The eluates were divided in two, resolved by sodium dodecyl sulfate-polyacrylamide gel electrophoresis, and electrotransferred onto duplicate polyvinylidene difluoride (PVDF) membranes. One PVDF membrane was immunoblotted for Ras, and the duplicate PVDF membrane was sprayed with En^{3}hance spray (Perkin Elmer), fluorographed at −70°C, and quantified by densitometry.

RESULTS

H-ras C181S localizes to the Golgi apparatus while mutant H-ras C184S traffics to the plasma membrane. To investigate whether the trafficking and membrane microlocalization of H-ras could be supported by a single palmitate, we generated GFP–H-rasG12V proteins with serine point mutations at Cys181 or Cys184. The resulting constructs, GFP–H-rasG12V C181S and H-rasG12V C184S, were expressed in BHK cells and visualized by confocal microscopy. Representative cells are shown in Fig. 1. The images show that dually palmitoylated GFP–H-rasG12V localized predominantly to the plasma membrane, with some decoration of the Golgi apparatus as reported previously (1, 8). In contrast, GFP–H-rasG12V C181S localized strongly to the Golgi apparatus with minimal staining of the plasma membrane. GFP–H-rasG12V C184S exhibited strong Golgi, ER, and plasma membrane staining. To examine whether the substantial Golgi pools of monopalmitoylated H-ras in BHK cells were due to delayed trafficking of newly synthesized protein, cells were pretreated with cycloheximide prior to imaging. Figure 1 shows that blocking new protein synthesis with cycloheximide resulted in loss of a background of diffuse ER staining evident in GFP–H-rasG12V C184S and to a lesser extent in GFP–H-rasG12V C181S expressing cells but accentuated the clear plasma membrane and Golgi localization, respectively, of these monopalmitoylated proteins. These results clearly show that palmitoylation of Cys181 (as in H-rasG12V C184S) is necessary and sufficient to traffic H-ras to the plasma membrane. In contrast, palmitoylation of Cys184 (as in H-rasG12V C181S) allows efficient trafficking through the exocytic pathway to the Golgi apparatus but is either unable to traffic H-rasG12V C181S beyond the Golgi apparatus and/or is less able to retain H-rasG12V C181S on the plasma membrane, resulting in a stable Golgi pool. Neither of the monopalmitoylated H-ras proteins exactly replicated the subcellular distribution of N-ras, which as reported previously (8), and shown in Fig. 1 is distributed between Golgi and plasma membrane pools that change little in cycloheximide-treated cells.

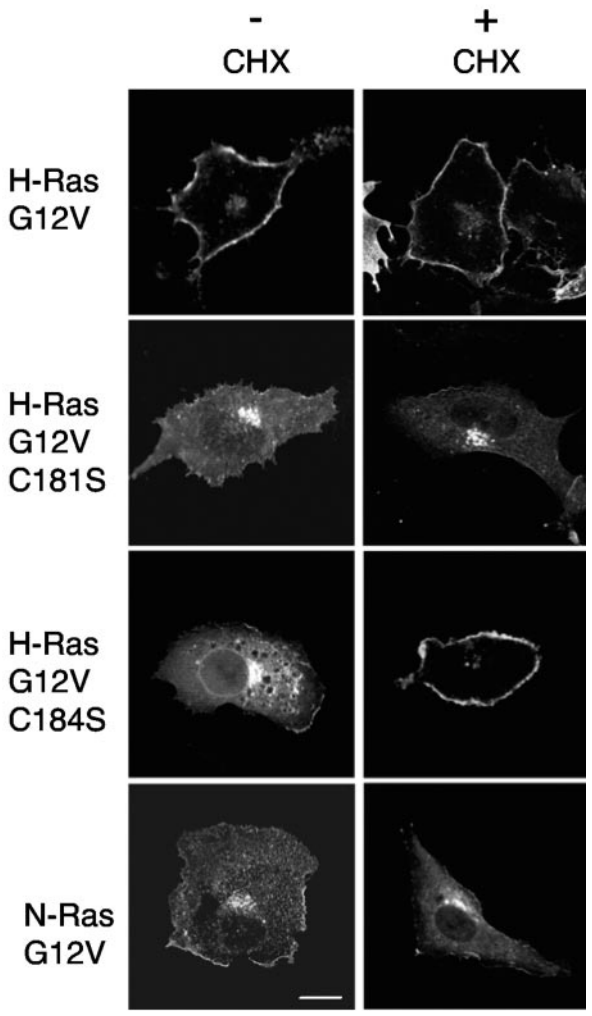

FIG. 1. H-ras palmitate groups play distinct roles in H-ras trafficking. BHK cells transiently expressing GFP–H-rasG12V, GFP–N-rasG12V, GFP–H-rasG12V C181S, or GFP–H-rasG12V C184S were imaged by confocal microscopy before (−) or after (+) incubation for 5 h in cycloheximide (CHX) to inhibit de novo protein synthesis. The disappearance of ER staining that is particularly striking with GFP–H-rasG12V C184S and to a lesser extent with GFP–H-rasG12V C181S was evident in all cells imaged. Similar distributions were seen when the same set of Ras proteins were expressed in COS cells (data not shown).

Inhibition of palmitoylation returns monopalmitoylated H-ras mutants to the ER. We next examined the role of palmitoyl

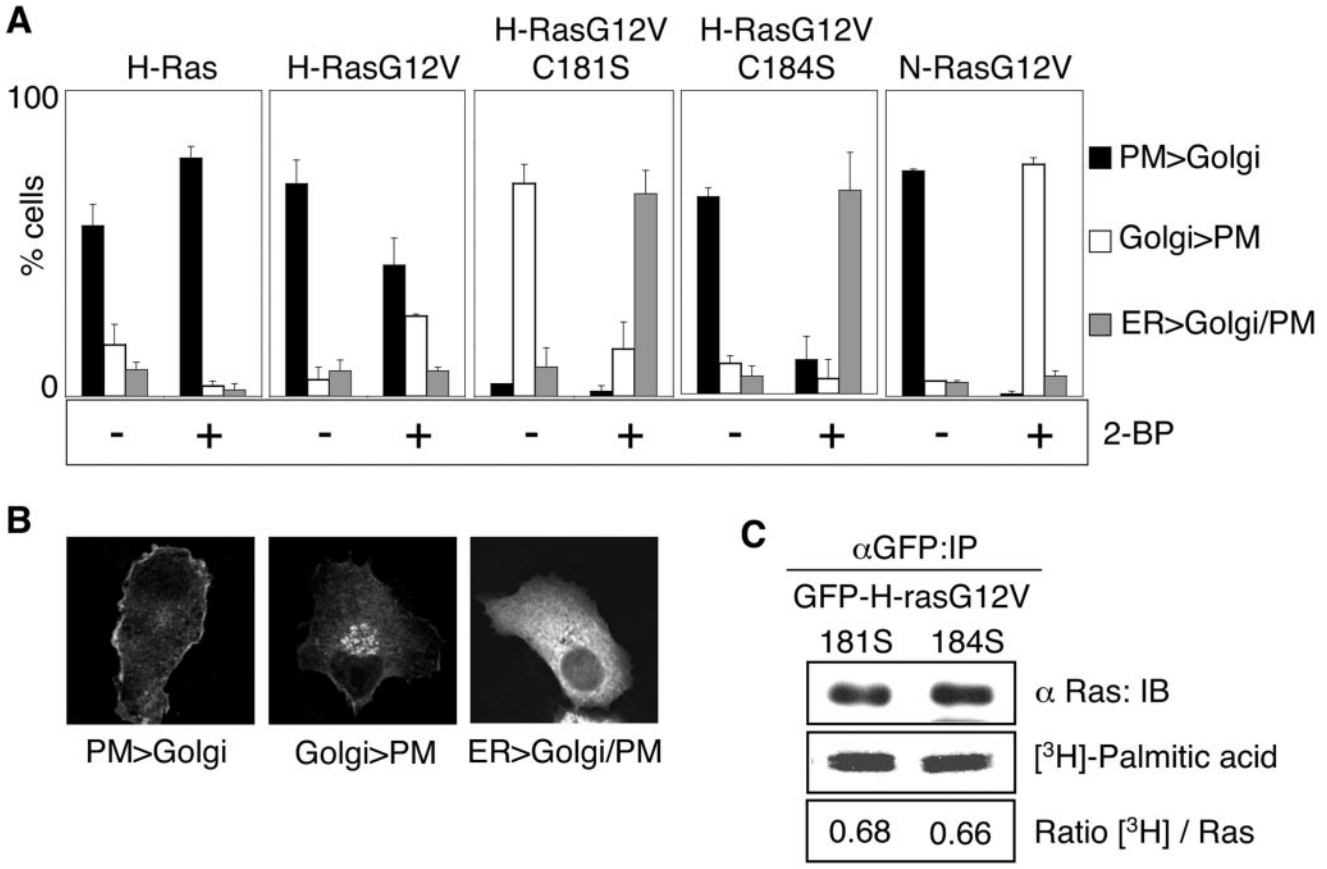

FIG. 2. Inhibiting palmitoylation causes redistribution of H-ras monopalmitoylated mutants to the ER. A. BHK cells stably transfected with GFP-ras proteins were pretreated for 2 h with cycloheximide to inhibit de novo protein synthesis. Cells were then incubated for 3 h in cycloheximide with or without 2-BP. The cells were visualized in a confocal microscope and scored for predominant plasma membrane (PM), Golgi, or endoplasmic reticulum (ER) localization. Examples of typical cells scored in these three categories are shown in panel B. At least 300 cells were evaluated from three independent experiments for each Ras protein. C. BHK cells transiently expressing GFP–H-rasG12V C181S or GFP–H-rasG12V C184S were labeled with [^{3}H]palmitic acid in the presence of cycloheximide. Duplicate anti-GFP immunoprecipitates prepared from whole-cell lysates were immunoblotted for Ras input and fluorographed for [^{3}H]palmitic acid. Blots and scans were quantified, and the ratio of [^{3}H]palmitic acid units per Ras unit was calculated. Representative blots and ^{3}H scans are shown. The ratios of [^{3}H]palmitic acid/Ras (in arbitrary units) for H-rasG12V C181S and H-rasG12V C184S, respectively, were 0.68 ± 0.01 and 0.66 ± 0.04 (means ± standard errors of the means, n = 3). IP, immunoprecipitation. IB, immunoblot.

transferase activity in maintaining the steady-state distribution of mono- and dually palmitoylated H-ras on the Golgi apparatus and plasma membrane. BHK cells expressing GFP–H-ras, GFP–H-rasG12V, GFP–H-rasG12V C181S, GFP–H-rasG12V C184S, or GFP–N-rasG12V were incubated in cycloheximide for 2 h to block new protein synthesis, and the incubation was then continued in cycloheximide for a further 3 h with or without 2-BP, an inhibitor of palmitoylation (9, 14, 56). Cells were visualized by confocal microscopy and scored for predominant plasma membrane, Golgi, or ER localization. Figure 2 shows that GFP–H-ras remained associated with the plasma membrane after 2-BP treatment, whereas 50% of cells expressing H-rasG12V showed a significant loss of plasma membrane staining, which was matched by a corresponding 40% of cells displaying a predominant increase in Golgi staining. These different responses to short-term inhibition of palmitoyl transferase are those that might be expected from the faster turnover of palmitate on GTP-loaded H-rasG12V compared to GDP-loaded GFP–H-ras (3). In contrast, monopalmitoylated GFP–H-rasG12V C184S relocalized from the plasma membrane and the Golgi apparatus to the ER and monopalmitoylated H-ras G12V C181S relocalized from the Golgi apparatus to the ER in response to 2-BP treatment. The redistribution of both monopalmitoylated H-ras proteins to the ER was not replicated by monopalmitoylated N-ras, which accumulated almost exclusively in the Golgi apparatus in 2-BP-treated cells. These differences in the subcellular distribution of monopalmitoylated H-rasG12V C181S and GFP–H-rasG12V C184S cannot be explained by differences in the stoichiometry of palmitoylation, because metabolic labeling with [^{3}H]palmitate showed equivalent incorporation of label into both mutant proteins (Fig. 2C).

Plasma membrane microlocalization of monopalmitoylated Ras proteins. We next visualized the microlocalization of dual- and monopalmitoylated GFP-ras on intact apical plasma membrane sheets using immunogold labeling and electron microscopy (EM). The immunogold patterns observed by EM were analyzed using Ripley's K-function, which reveals whether the

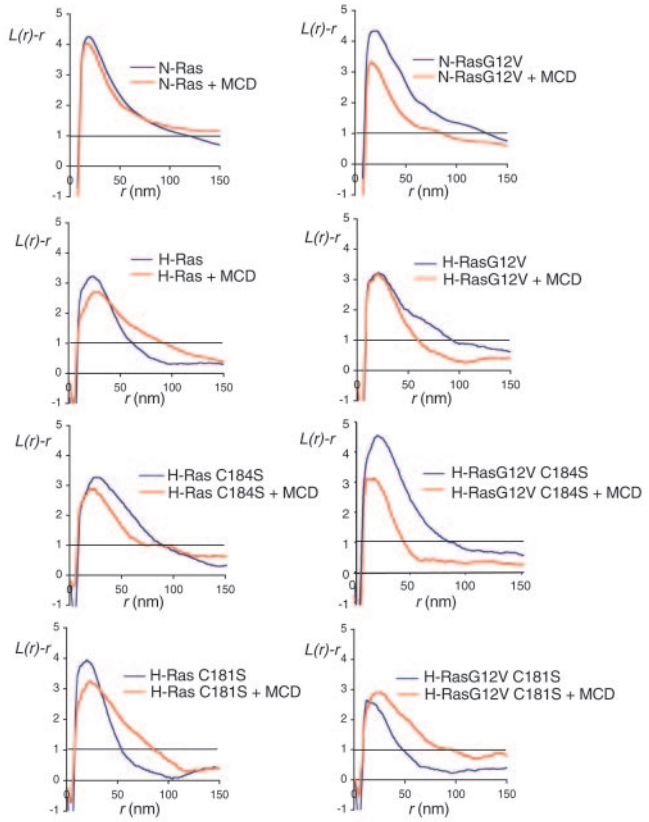

FIG. 3. The plasma membrane microlocalization of monopalmitoylated H-rasG12V C184S emulates that of GFP–N-rasG12V. Apical plasma membrane sheets from BHK cells transiently expressing GFP-ras proteins were labeled with anti-GFP antibodies coupled directly to 4-nm gold. Where indicated, cells were incubated with 1% β-methylcyclodextrin for 30 min to deplete cell surface cholesterol. The immunogold point patterns were analyzed using Ripley's K-function. The graphs show weighted mean K-functions (n = 8 to 17 sheets) standardized on the 99% confidence interval (CI) for complete spatial randomness. The average number of gold particles per plasma membrane sheet evaluated was 939 μm^{-2}. In this analysis a pattern is significantly clustered if the $L(r) - r$ curve leaves the CI (i.e., is >1), whereas in a random pattern the $L(r) - r$ approximates to 0 for all values of r (for examples see references 37 and 42). Differences between control and cholesterol-depleted membranes were evaluated for each construct using bootstrap tests. A statistically significant effect of cholesterol depletion is seen on the clustering of GFP–H-ras (P = 0.017), GFP–N-rasG12V (P = 0.039), and GFP–H-rasG12V C184S (P = 0.001).

pattern is significantly clustered or random. We have shown previously using this methodology that GFP–H-rasG12V exists in small clusters on the plasma membrane that are unaffected by cholesterol depletion (42). Figure 3 shows that GFP–H-rasG12V C184S and GFP–H-rasG12V C181S clustered to the same extent as GFP–H-rasG12V. Although the overall labeling density of GFP–H-rasG12V C181S on the plasma membrane sheets was lower than the other H-ras proteins, it was sufficient for immunogold point pattern analysis (which does not depend on labeling density) (40). The clustering of GFP–H-rasG12V and GFP–H-rasG12V C181S proteins was not significantly affected by cholesterol depleting the cells prior to preparation of the membrane sheets. Thus, a single palmitate on Cys184 appears to be sufficient to microlocalize H-ras to cholesterol-independent nonraft clusters. In striking contrast, the clustering of GFP–H-rasG12V C184S was significantly reduced in cholesterol-depleted cells (Fig. 3), indicating that a single palmitate on Cys181 supports the association of H-rasG12V with cholesterol-dependent microdomains. We next examined the spatial distribution of GFP–N-rasG12V, which is also anchored by a single palmitate on Cys181 and found the same result: the clustering of GFP–N-rasG12V was significantly decreased in cholesterol-depleted cells (Fig. 3).

The observation that H-rasG12V monopalmitoylated on Cys181 (H-rasG12V C184S) was sufficient to allow association with lipid rafts was unexpected. We therefore looked for corresponding changes in the microlocalization of wild-type H-ras C184S. Figure 3 shows that the clustering of dually palmitoylated wild-type H-ras was significantly decreased in cholesterol-depleted cells, as reported previously (42), consistent with inactive GDP-loaded H-ras segregating to lipid rafts. In contrast, the clustering of GDP-loaded H-ras C184S and GDP-loaded N-ras was unaffected by cholesterol depletion (Fig. 3). These data suggest that whereas H-ras loses affinity for lipid raft domains on GTP-loading, N-ras and monopalmitoylated H-ras C184S behave in exactly the opposite manner and increase affinity for lipid rafts on GTP loading. We conclude that once delivered to the plasma membrane, a single palmitate on Cys184 is sufficient to microlocalize H-rasG12V to cholesterol-independent nonraft microdomains. Conversely, a single palmitate on Cys181 changes the microlocalization of H-ras such that it mimics the microlocalization of N-ras.

Effect of palmitoylation on the dynamics of H-ras plasma membrane interactions. The dynamics of plasma membrane association of the same set of GFP-ras proteins was examined in living cells by fluorescence recovery after photobleaching (FRAP). We first compared the fluorescence recovery of GFP–H-rasG12V and GFP–H-rasG12V C181S in the plasma membrane. Typical FRAP curves are shown in Fig. 4A, and the averaged results are depicted in Fig. 4B. In keeping with our previous results (35), GFP–H-rasG12V had a characteristic fluorescence recovery time (τ; the time required to attain half of the recoverable fluorescence intensity for a Gaussian bleach profile) (2) of ~0.4 s with a laser beam of 0.85-μm Gaussian radius (Fig. 4A). The fluorescence recovery of GFP–H-rasG12V C181S was faster (τ, ~0.2 s; Fig. 4A and B). Importantly, the amounts of the H-rasG12V C181S detected in the plasma membrane were sufficient to allow accurate FRAP measurements, although GFP–H-rasG12V C181S is localized mainly at the Golgi apparatus (Fig. 1). In addition, the fluorescence recovery of cytoplasmic GFP (Fig. 4A) occurs on a very fast time scale ($\tau < 0.005$ s) that is more than an order of magnitude faster than that of GFP–H-rasG12V C181S. This indicates that free diffusion in the cytoplasm does not contribute significantly to the measurements of the GFP–H-ras mutants. The relatively fast fluorescence recovery of GFP–H-rasG12V C181S reflects weaker interactions of the mutant with the plasma membrane. Such weak interactions are often a characteristic of proteins that undergo exchange between membrane and cytoplasmic pools. They may also characterize proteins that are stably associated with the plasma membrane yet diffuse laterally at a relatively fast rate. To discriminate between these characteristics we performed FRAP measurements with

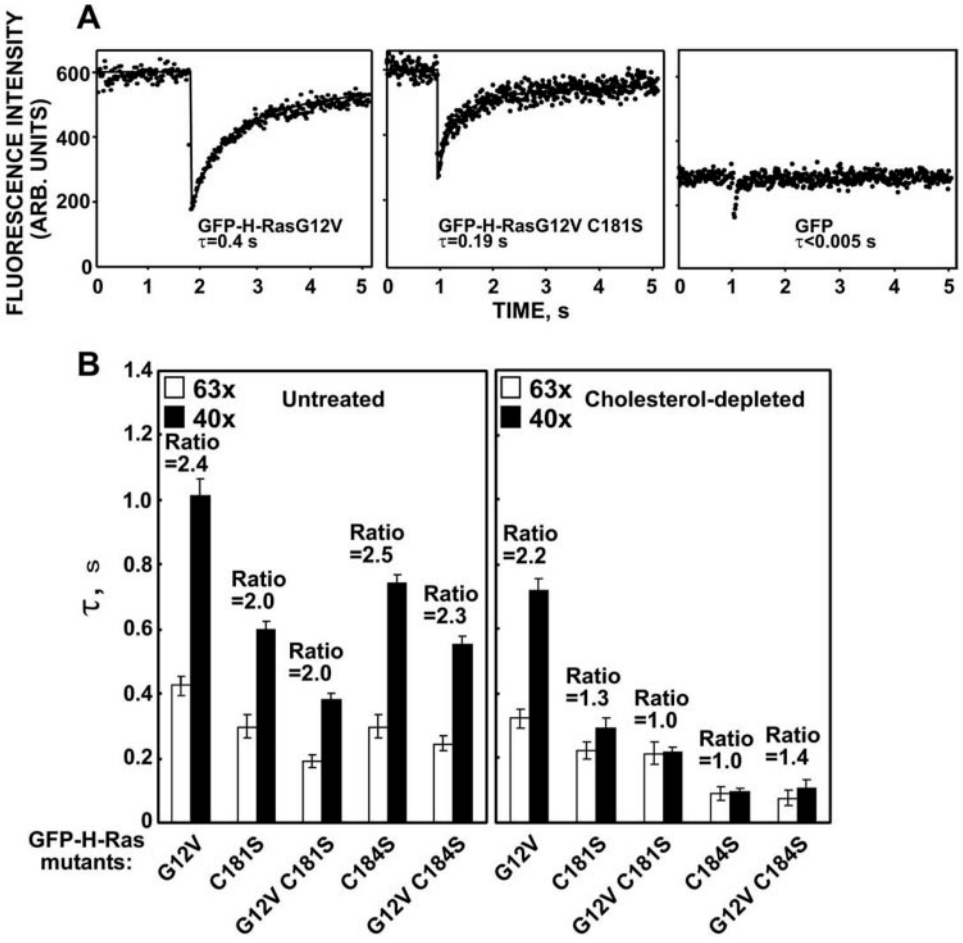

FIG. 4. Monopalmitoylated Ras proteins exhibit different dynamic interactions with the plasma membrane than dual-palmitoylated H-ras. A. FRAP experiments (with a 63× objective) were conducted on COS-7 cells transiently expressing the depicted GFP constructs. The dots represent the fluorescence intensity. Solid lines show the best fit of a nonlinear regression analysis. GFP exhibits free diffusion in the cytoplasm, resulting in extremely fast fluorescence recovery. Thus, free diffusion in the cytoplasm occurs on a faster time scale and does not contribute significantly to the measurements depicted for GFP–H-rasG12V and GFP–H-rasG12V C181S. B. FRAP measurements were also performed in untreated and in cholesterol-depleted cells using two beam sizes that were generated by 63× and 40× objectives. The fluorescence recovery time (τ) determined with each objective and the $\tau(40\times)/\tau(63\times)$ ratios derived (means ± standard errors of the means of 15 to 60 measurements) are shown. The mobile fractions were high for all proteins (>90%). We used *t* tests to determine whether the ratios differed significantly from that expected for pure lateral diffusion, an experimentally determined ratio between the areas illuminated by the laser beam using the two objectives (means ± standard errors of the means value of 2.56 ± 0.30, $n = 39$). ARB., arbitrary.

laser beams of different size (13, 25, 34). If FRAP occurs by lateral diffusion, τ is essentially the characteristic diffusion time, τ_D, and is proportional to the area illuminated by the beam ($\tau_D = \omega^2/4D$, where ω is the Gaussian radius of the laser beam). If FRAP occurs by dynamic exchange between membrane-bound and cytosolic pools, τ reflects the chemical relaxation time due to exchange, which is equal on all surface regions regardless of whether they are illuminated by the beam and therefore does not depend on the beam size (13, 25, 34). The expected ratio between $\tau(40\times)/\tau(63\times)$ for the two beam sizes generated using 40× and 63× objectives is 2.56 for pure lateral diffusion or 1 (no dependence on beam size) for pure exchange. In agreement with our earlier results (34), GFP–H-rasG12V exhibited pure lateral diffusion, evident by a $\tau(40\times)/\tau(63\times)$ ratio of 2.4, not significantly different from the ratio between the beam sizes ($P > 0.1$ in a Student's two-tailed *t* test; Fig. 4B). By contrast, GFP–H-rasG12V C181S exhibited a mixed mode of fluorescence recovery (contribution of both lateral diffusion and exchange), as indicated by the $\tau(40\times)/\tau(63\times)$ ratio of 2.0, significantly different from either 1 or 2.56 (Fig. 4B, $P < 0.001$). Similar results were obtained with GFP–H-ras C181S for which the $\tau(40\times)/\tau(63\times)$ ratio was 2.0 as well (Fig. 4B). These results indicate that palmitate on cysteine 181 is essential for stable membrane association of both GDP- and GTP-bound H-ras, since its absence in GFP–H-ras C181S or in GFP–H-rasG12V C181S resulted in exchange between the plasma membrane and cytosolic pools. Interestingly, GFP–H-ras C184S and GFP–H-rasG12V C184S exhibited, respectively, $\tau(40\times)/\tau(63\times)$ ratios of 2.5 and 2.3 similar to that of GFP–H-rasG12V ($P > 0.1$, Fig. 4B). We conclude that palmitate on Cys181, but not palmitate on Cys184, is sufficient for stable membrane interactions of H-ras.

To examine the contribution of each of the palmitate moieties to the interactions of H-ras with cholesterol-dependent and cholesterol-independent microdomains, we studied by FRAP the effects of cholesterol depletion on the membrane affinity of the mutants. Cholesterol depletion was performed as detailed previously (35). GFP–H-rasG12V exhibited fluorescence recovery by pure lateral diffusion in the cholesterol-depleted cells with a $\tau(40\times)/\tau(63\times)$ ratio of 2.2, close to the value obtained for GFP–H-rasG12V in untreated cells ($P > 0.1$, Fig. 4B). Cholesterol depletion had, however, a strong impact on membrane association of all palmitate mutants; whose fluorescence recovery shifted from the mode of lateral diffusion or mixed lateral diffusion and exchange to pure or almost pure exchange. Thus, the $\tau(40\times)/\tau(63\times)$ ratios of GFP–H-rasG12V C181S and GFP–H-ras C184S were 1.0, as expected for pure exchange; the ratio for GFP–H-ras C181S and GFP–H-rasG12V C184S was 1.3 to 1.4, suggesting almost pure exchange with a minor contribution of lateral diffusion (Fig. 4B), but even for these latter mutants the measured ratios are not significantly different from 1 ($P > 0.2$). Importantly, in the cholesterol-depleted cells the exchange rates of GFP–H-ras C181S and of GFP–H-rasG12V C181S were significantly slower (τ, ~0.2 s) than those of GFP–H-ras C184S and GFP–H-rasG12V C184S (τ, ~0.1 s). The difference in the τ values gained a clear statistical significance ($P < 0.05$, Fig. 4B). These results indicate that the palmitate on Cys184 contributes more than the palmitate on Cys181 to the association of H-ras with cholesterol-independent microdomains, in line with the clustering analysis, which showed that the single palmitate on cysteine 184 is sufficient to correctly microlocalize H-ras to such domains.

We correlated the FRAP estimates of membrane affinity with steady-state distributions between soluble and membrane pools. To this end, we determined the proportion of wild-type H-, N-, and mutant H-ras proteins recovered in membrane (P100) and cytosolic (S100) fractions. Figure 5 shows that both H-ras single acylation mutants as well as N-ras have a greater proportion of cytosolic protein than wild-type H-ras, suggesting that dual acylation confers a stronger association with cellular membranes than monoacylation.

Golgi apparatus-localized Ras and plasma membrane-localized Ras vary in their ability to activate Raf, MEK, and ERK. Finally, we compared the efficiencies with which the monopalmitoylated H-rasG12V and dually palmitoylated H-rasG12V activate Raf. First, we assayed Raf recruitment using the Ras binding domain of Raf (isolated Raf-RBD) coupled to mRFP (mRFP-RBD). Figure 6A shows that coexpression of GFP–H-rasG12V or GFP–H-rasG12V C184S in BHK cells recruited mRFP-RBD from the cytosol predominantly to the plasma membrane and to a much lesser extent the Golgi apparatus. In contrast, GFP–H-rasG12V C181S recruited mRFP-RBD almost exclusively to the Golgi apparatus. GFP–N-rasG12V recruited mRFP-RBD to both the plasma membrane and Golgi apparatus. Thus, the redistribution of the mRFP-RBD probe closely matches the subcellular distribution of the respective Ras proteins. We next measured mRFP-RBD redistribution from cytosol (S100 fraction) to membrane (P100 fraction) using quantitative immunoblotting of fractionated BHK cells. Although the three monopalmitoylated Ras proteins recruited Raf with near equal efficiency to the Golgi apparatus or plasma membrane, H-rasG12V C181S and N-rasG12V were significantly less potent at stimulating Raf kinase activity than H-rasG12V C184S (Fig. 7A). There was no difference in the specific activity of Raf recruited and activated by H-rasG12V and H-rasG12V C184S. The Raf activation profile of the set of H-ras proteins was also replicated in Erk activation and PC12 cell differentiation assays, although in both these assays N-rasG12V was equipotent with H-rasG12V (Fig. 7B and C). We conclude that RasG12V proteins activate Raf-1 less efficiently on the Golgi apparatus than on the plasma membrane, accounting for the lower specific activity of Raf-1 activated by H-rasG12V C181S and N-rasG12V compared with H-rasG12V and H-rasG12V C184S. Nevertheless, the Golgi platform from which N-ras operates is more efficient at coupling Raf activation to Erk activation than the Golgi platform utilized by H-rasG12V C181S.

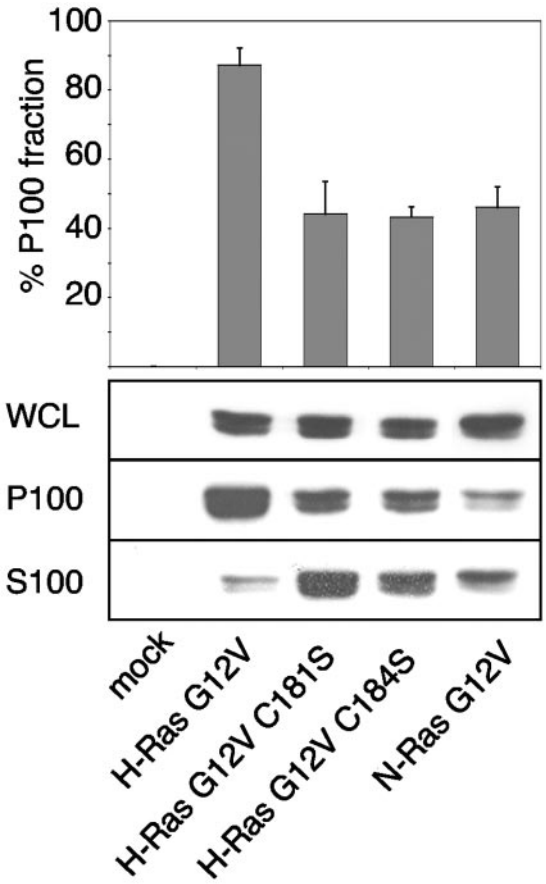

FIG. 5. Monopalmitoylated Ras proteins have a reduced affinity for the plasma membrane. BHK cells expressing Ras proteins were fractionated into S100 and P100 fractions and immunoblotted to determine the relative extent of membrane association. The graph shows the percentage of Ras protein associated with the P100 fraction (means ± standard errors of the means, $n = 3$). WCL, whole-cell lysates.

DISCUSSION

In this study we show that the trafficking, plasma membrane affinity, and microlocalization of doubly palmitoylated H-ras is substantially different from monopalmitoylated H-ras. We fur-

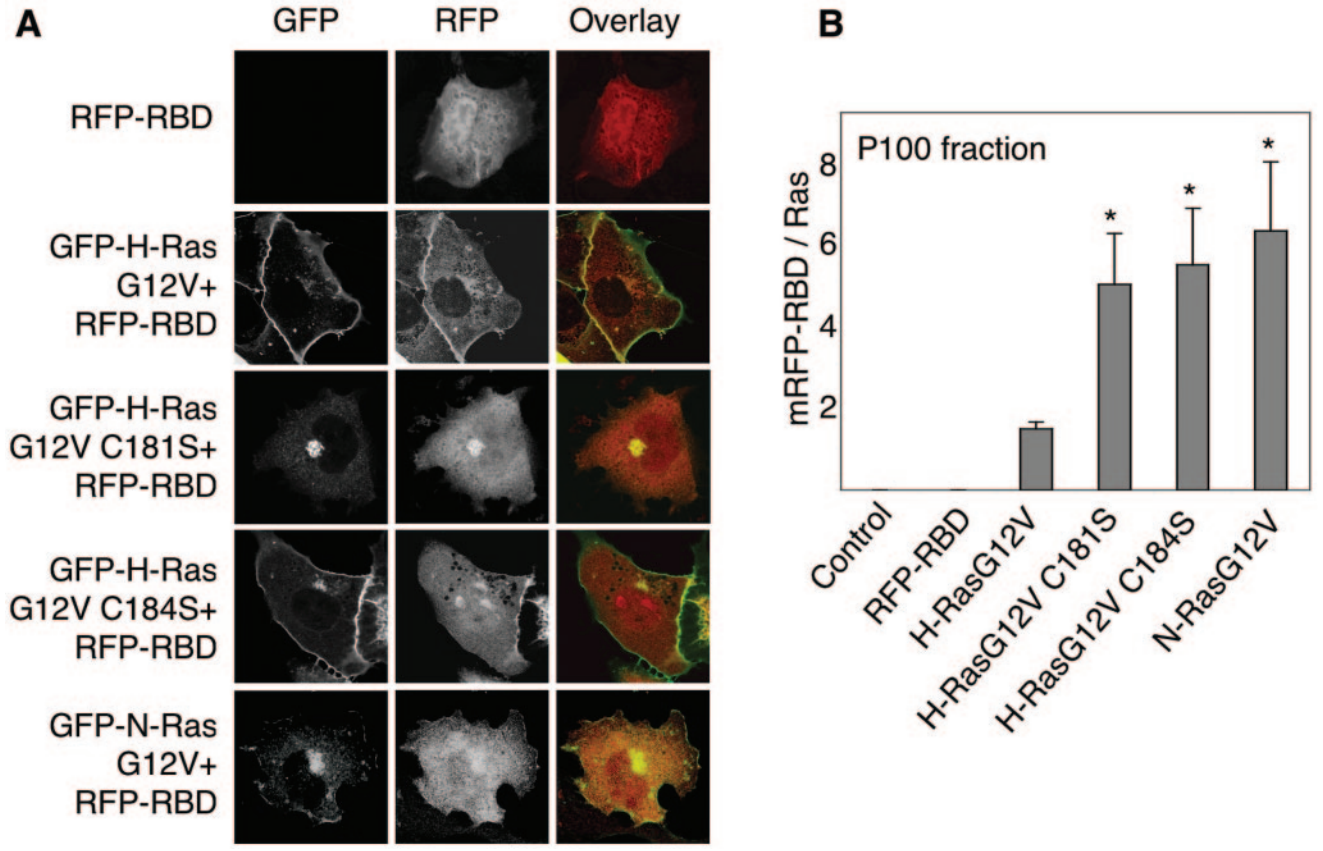

FIG. 6. Monopalmitoylated RasG12V proteins recruit Raf to membranes more efficiently than H-rasG12V. A. BHK cells coexpressing GFP-ras proteins and mRFP-RBD were incubated for 5 h in cycloheximide and visualized by confocal microscopy. Representative cells are shown. B. BHK cells transiently expressing GFP-ras proteins and mRFP-RBD were fractionated into membrane (P100) and cytosolic (S100) fractions by high-speed centrifugation. GFP-ras and mRFP-RBD content of the P100 fraction was estimated using quantitative immunoblotting. The graphs show mRFP-RBD recruitment per unit of Ras expressed in arbitrary phosphorimager units (means ± standard errors of the means, $n = 3$). Significant differences from control (H-rasG12V), evaluated in t tests, are shown on the graph (an asterisk indicates P value of <0.05).

ther show by comparing two different monopalmitoylated H-ras mutants that the spacing of palmitate with respect to the farnesylated C-terminal cysteine has a profound effect on trafficking and plasma membrane interactions. Finally, we show that a monopalmitoylated H-ras mutant with the same prenyl-palmitate spacing as N-ras behaves as a phenocopy of N-ras in many aspects of its membrane interactions. Overall the study yields intriguing new insights into how prenylated-palmitoylated anchors operate and control the subcellular microlocalization of the attached protein. We use three complementary techniques to elucidate palmitate function: immunofluorescence to monitor subcellular distribution, FRAP to measure plasma membrane affinity, and EM to map plasma membrane microlocalization (Table 1).

Role of palmitates in trafficking. H-ras with a Cys184 monopalmitoylated anchor (H-ras C181S) is confined mainly to the Golgi apparatus and is only inefficiently delivered to the plasma membrane. The Golgi pool of H-ras C181S is stable

TABLE 1. Summary of results[a]

Protein	Palmitoylated cysteine(s) in the membrane anchor	Localization	Localization after 2-BP treatment	Cholesterol-dependent nanoclustering	Affinity for PM	Affinity for PM after cholesterol depletion
H-ras	Cys181 and Cys184	PM≫Golgi	PM	Yes	+++	+++
H-ras G12V	Cys181 and Cys184	PM≫Golgi	PM=Golgi	No	+++	+++
H-ras C181S	Cys184	Golgi≫PM	nd	No	++	+
H-ras G12V C181S	Cys184	Golgi≫PM	ER	No	++	+
H-ras C184S	Cys181	PM>Golgi	ND	No	+++	+
H-ras G12V C184S	Cys181	PM>Golgi	ER	Yes	+++	+
N-ras	Cys181	PM=Golgi	ND	No	ND	ND
N-ras G12V	Cys181	PM=Golgi	Golgi	Yes	ND	ND

[a] The first four columns summarize data presented in Fig. 1 to 3. Columns 4 and 5 show affinity of Ras proteins for the plasma membrane (PM) before and after cholesterol depletion as measured by FRAP: +++, ++, and + represent $\tau(40\times)/\tau(63\times)$ ratios of 2.5 to 2.01, 2.0 to 1.5, and <1.5, respectively. ND, not determined.

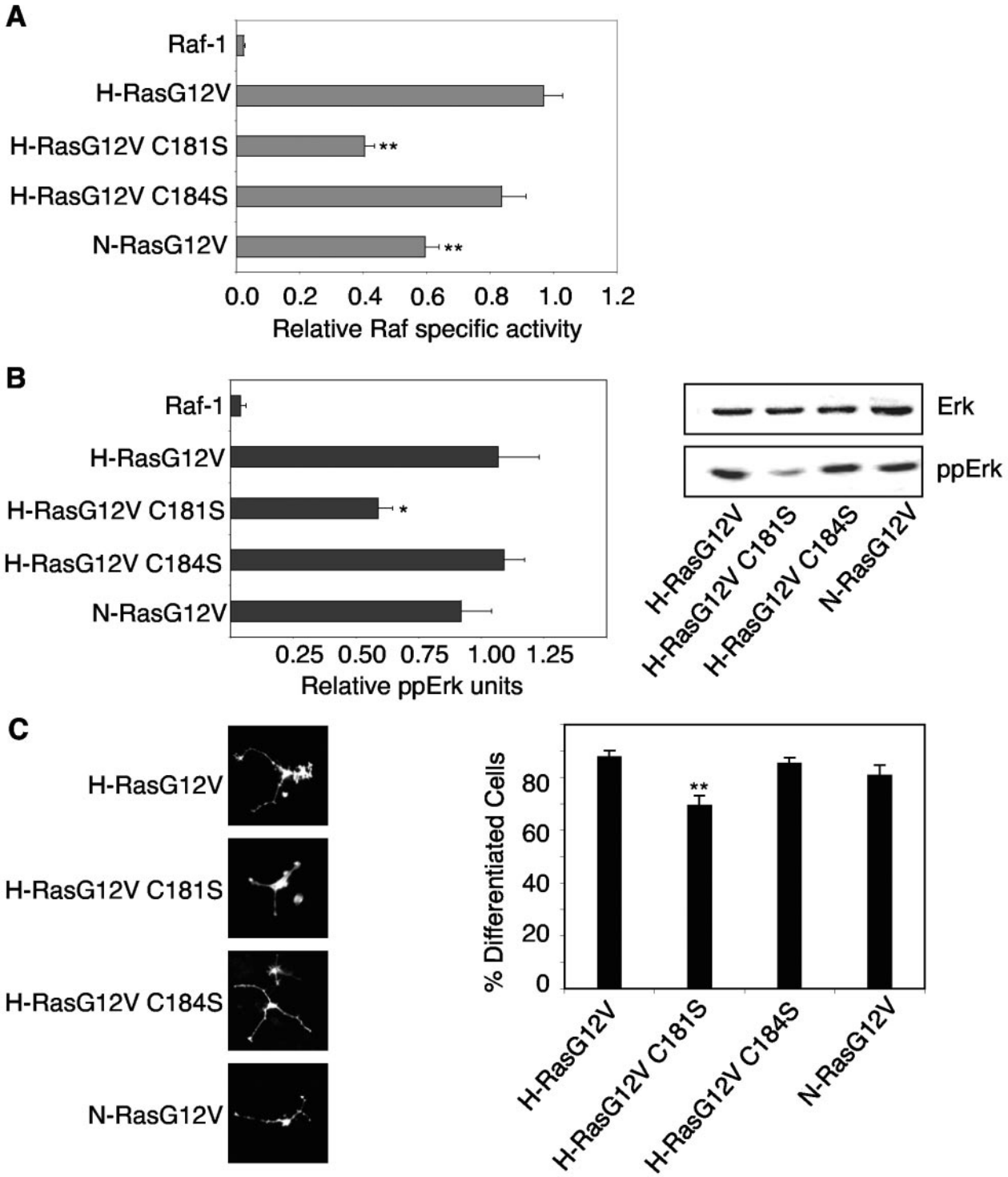

FIG. 7. Monopalmitoylated RasG12V proteins activate the Raf/MEK/MAPK cascade with varying efficiencies. A. P100 fractions from BHK cells transiently expressing equivalent amounts of H-rasG12V, N-rasG12V, H-rasG12V C181S, or H-rasG12V C184S were assayed for Raf activity in a coupled mitogen-activated protein kinase assay with myelin basic protein phosphorylation as a read out (49). P100 fractions were immunoblotted for Raf-1, and the kinase assay results were standardized on the Raf content of the P100 fraction to estimate Raf-1-specific activity. The graph shows Raf specific activity (means ± standard errors of the means, $n = 3$) expressed relative to the activity of Raf-1 recruited and activated by H-rasG12V. B. The same lysates assayed in panel A for Raf activity were analyzed for Erk activation by quantitative immunoblotting for phosphorylated Erk (ppErk). A representative blot is shown, and the graph shows results (means ± standard errors of the means, $n = 3$) for three independent experiments. Significant differences from control (H-rasG12V), evaluated in t tests, are shown on the graph (*, $P < 0.05$). C. PC12 cells transiently expressing GFP-ras proteins were visualized 72 h after transfection by fluorescence microscopy. The percentage of GFP-positive, differentiated cells (with neurite outgrowth of at least twice the diameter of the cell body) was estimated by counting >300 cells per construct per experiment. Images of differentiated cells are shown. The graph shows results obtained from three independent experiments (means ± standard errors of the means, $n = 3$). Significant differences from control (H-rasG12V), evaluated in t tests, are shown on the graph (**, $P < 0.01$).

and does not simply represent newly synthesized protein because it is not diminished when new protein synthesis is inhibited. In contrast, H-ras with a Cys181 monopalmitoylated anchor (H-ras C184S) is efficiently delivered to the plasma membrane with little Golgi pooling. The steady-state distribution of these monopalmitoylated H-ras proteins in BHK and COS cells reported here matches those seen in MDCK cells (47). The Golgi localization and plasma membrane localization of H-ras C181S and H-ras C184S are both dependent on palmitoylation, because blocking palmitoylation returns both proteins to the ER, reflecting the endomembrane targeting function of an isolated processed CAAX box (8). These data suggest that palmitoylation of Cys184 in the ER only supports efficient trafficking as far as the Golgi apparatus and not beyond to the plasma membrane, whereas palmitoylation of Cys181 supports ER-to-Golgi transport but is required, and is sufficient, for efficient Golgi-to-plasma membrane trafficking. Thus, these two monopalmitoylated H-ras proteins appear to be differentially sorted within the Golgi apparatus for onward transport to the plasma membrane. A similar requirement for palmitoylation of a specific cysteine residue for post-Golgi transport has also been reported for the GAD65 protein (28). It is not possible to ascribe these results to different rates of palmitate turnover because these are the same ($t_{1/2} \leq 15$ min) on both H-ras C181S and H-ras C184S (31). Moreover, the rate of recycling of H-ras, N-ras, H-ras C181S, and H-ras C184S between plasma membrane and Golgi apparatus has recently been measured in live cells (47). Palmitoylated Ras proteins undergo depalmitoylation on the plasma membrane and retrograde transport to the Golgi apparatus by a mechanism that does not involve vesicular transport (47). The rate of retrograde transport for dually palmitoylated H-ras is much slower ($t_{1/2} = 6$ min) than for monopalmitoylated N-ras ($t_{1/2} = 1.1$ min) and faster still for monopalmitoylated H-ras C184S ($t_{1/2} = 41$s) and H-ras C181S ($t_{1/2} = 38$s) (47). The similar rates of retrograde transport of H-ras C184S and H-ras C181S again argue in favor of a significant problem with forward transport of H-ras C181S from the Golgi apparatus to plasma membrane to account for the low level of plasma membrane localization of H-ras C181S compared to H-ras C184S. It is plausible, however, that the somewhat weaker affinity for the plasma membrane of H-ras C181S compared to H-ras C184S (Fig. 4) accounts for the slightly faster retrograde transport of H-ras C181S from the plasma membrane to the Golgi apparatus (47) and contributes to the large Golgi pool of H-ras C181S.

Interestingly, blocking palmitoylation resulted in a partial relocalization of H-rasG12V to the Golgi apparatus rather than the ER. We account for this observation by proposing that on dually palmitoylated H-ras, thioesterases may have an easier access to Cys181-palmitate than Cys184-palmitate; if so, when Cys181-palmitate is removed, H-ras remains tethered by an anchor equivalent to that on H-ras C181S, which is unable to exit the Golgi apparatus. Two studies provide support for this proposal. First, a structure of the N-ras anchor in contact with a lipid bilayer shows that Cys181 is not fully buried in the membrane and the thioester bond is accessible to water (15). In contrast, the side chain of Leu184 on N-ras is deeply buried and contributes significantly to the membrane affinity of the N-ras anchor (15). If the palmitate on Cys184 is equally buried, then in the dually palmitoylated H-ras protein the Cys184 palmitate could be partially protected from hydrolysis. Second, this protection from hydrolysis would probably only hold for as long as Cys181 is palmitoylated; this type of sequential depalmitoylation of H-ras could account for the complex, two-component decay kinetics for palmitate turnover on H-rasG12V recently described (3). We also suggest that it is the increased membrane affinity provided by Leu184 that allows depalmitoylated N-ras to traffic to the Golgi apparatus after presumably being initially targeted back to the ER like H-ras C184S. In support of this role for Leu184 as an important determinant of N-ras anchoring, a recent study has shown that H-ras C184L operates as a very close biological mimic of N-ras in Jurkat cells; the modified anchor supports H-ras C184L activation and signaling on the Golgi apparatus in response to low-grade T-cell-receptor activation, whereas this stimulus normally only activates N-ras (38).

The more extensive Golgi localization of N-rasG12V and H-rasG12V C181S compared with H-rasG12V and H-rasG12V C184S correlated with a reduced efficiency to activate Raf-1, suggesting that the Golgi apparatus may be a suboptimal environment for Raf activation. This reduced Raf-1 activity was translated into reduced Erk activation in cells expressing H-rasG12V C181S but not in cells expressing N-rasG12V, where Erk activation was robust. A possible conclusion from these data is that the scaffolding of the Raf/MEK/Erk cascade in the Golgi microenvironment of N-rasG12V is more efficient or stable than in the Golgi microenvironment of H-rasG12V C181S. Taken together these data therefore argue for differential lateral segregation of N-rasG12V and H-rasG12V C181S to different microdomains of the Golgi apparatus, in turn perhaps due to the absence of Leu184 in the mutant H-ras protein. Interestingly, all of the monopalmitoylated RasG12V proteins recruited more mRFP-RBD to cell membranes than dually palmitoylated GFP–H-rasG12V, suggesting that the effector domain on monopalmitoylated Ras proteins might be more accessible or that the interaction of the Raf-RBD with monopalmitoylated Ras proteins is more stable than with dually palmitoylated H-rasG12V. How the membrane anchor might influence Ras effector binding, as suggested by these data, is unclear but merits further investigation (20).

Role of palmitates in plasma membrane binding and lateral segregation. H-rasG12V has a high-affinity interaction with the plasma membrane reflected in FRAP by pure lateral diffusion (48). This interaction is predominantly with cholesterol-independent microdomains, also called nanoclusters, that operate as signaling platforms (20). The C-terminal anchor, protein sequences within the adjacent hypervariable region, and G domain contribute to this microlocalization. The delivery of H-rasG12V C181S to the plasma membrane is significantly impeded by defective trafficking, but once at the plasma membrane H-rasG12V C181S clusters in cholesterol-independent domains to a similar extent as H-rasG12V. The overall affinity of H-rasG12V C181S for the plasma membrane, however, is lower than H-rasG12V (Table 1). Combining these results, we suggest that an anchor of palmitate on Cys184 is sufficient to target H-rasG12V C181S to cholesterol-independent nanoclusters, but the interaction of H-rasG12V C181S with these clusters, as well as interactions with the bilayer outside of

clusters, is weaker. The affinity of GDP-loaded H-ras C181S for the plasma membrane is also reduced compared to H-ras but clusters in cholesterol-dependent domains (Table 1). Overall, after allowing for the substantial decrease in membrane affinity flowing from the presence of a single palmitate, the basic regulation of lateral segregation supported by the dually palmitoylated H-ras anchor seems largely intact with a Cys-184 monopalmitoylated anchor.

In contrast, the Cys-181 monopalmitoylated anchor dramatically reverses the lateral segregation of H-ras C184S and H-rasG12V C184S compared to the cognate dually palmitoylated proteins. Thus, a Cys-181 monopalmitoylated anchor supports clustering of H-ras, but GDP-loaded H-ras C184S associates with cholesterol-insensitive clusters whereas GTP-loaded H-rasG12V C184S segregates to cholesterol-sensitive clusters (Table 1). A second difference from the Cys-184 monopalmitoylated anchor is that the Cys-181 monopalmitoylated anchor provides much higher affinity for the plasma membrane (Table 1). Thus, the increased spacing of the Cys181-palmitate from the prenyl group increases the affinity of the anchor for the membrane, indicating that affinity does not simply reflect the total hydrophobicity provided by the lipid moieties. This observation can in part be rationalized again in the light of work on the N-ras anchor peptide, which shows that palmitate and prenyl groups at Cys181 and Cys186 results in the intervening peptide being inserted deeply into the bilayer (15). This allows additional hydrogen bonding between peptide side chains and lipid head groups to provide additional membrane affinity. We speculate that the monoCys181-palmitate anchor on H-ras in part mimics the N-ras anchor peptide insertion and thus gains increased membrane affinity by a mechanism that is not available to the monoCys184-palmitate anchor. Consistent with this hypothesis we show here that the nanoclustering of N-ras on the plasma membrane emulates that of the H-ras C184S protein. Clustering of GDP-loaded N-ras is cholesterol independent, whereas a significant fraction of GTP-loaded N-ras is clustered in cholesterol-sensitive domains. One important inference from this observation is that N-ras may be the Ras isoform that is "designed" to activate effectors from within lipid rafts. A more general conclusion is that not only the specific lipids comprising the anchor but also their spacing and the intervening peptide backbone will determine the preferred membrane environment of a C-terminal anchor. It is interesting to note that the N-terminal anchors of the Src family kinases comprise myristate plus multiple iterations of one or more palmitates with different intervening peptide sequences. The experiments with Ras reported here would argue that these Src family kinase anchors on Fyn, Lyn, and Lck are likely to exhibit different preferences for their lipid environments.

A striking result from the FRAP analysis shows that cholesterol depletion dramatically reduces the membrane affinity of all of the monopalmitoylated H-ras proteins, in contrast to dually palmitoylated H-ras, which is minimally affected (Table 1). The simplest interpretation of this result is that all stable plasma membrane interactions of monopalmitoylated proteins require a direct or indirect interaction of the anchor with cholesterol. This membrane affinity function of cholesterol is separable from the role of cholesterol in promoting clustering of membrane-anchored proteins that is measured by EM mapping. There is no time dimension to the EM analysis, which in effect simply takes a snapshot of proteins attached to the plasma membrane at the time of assay. On the other hand, FRAP beam size-dependent studies measure the overall affinity of the protein to the membrane, providing evidence for an effect of cholesterol on the "vertical" distribution between membrane-associated and cytoplasmic pools. The combination of FRAP and EM therefore reveals that lateral segregation of lipid-anchored proteins into cholesterol-sensitive and -insensitive domains can be imposed on proteins with low overall affinity for the plasma membrane. The specific role of cholesterol in providing membrane affinity for monopalmitoylated proteins also suggests the intriguing possibility that the anchor of these proteins could directly interact with cholesterol irrespective of how they are laterally segregated.

In summary, we show here that the two palmitates in the C-terminal anchor of H-ras serve distinct functions. Cys184-palmitate is dominant for determining H-ras lateral segregation, whereas Cys181-palmitate is critical for efficient trafficking from the Golgi apparatus to the plasma membrane. Acting together, the two palmitates increase the membrane affinity of H-ras and somewhat paradoxically render membrane-binding affinity independent of cholesterol. The study shows that both the stoichiometry of palmitoylation and the spatial organization of individual palmitates are important functional characteristics of membrane anchors.

ACKNOWLEDGMENTS

This work was supported by grants from the National Institutes of Health (GM-066717) and the National Health and Medical Research Council to J.F.H. and R.G.P. I.A.P. is a Royal Society University Research Fellow. Y.I.H. is an incumbent of the Zalman Weinberg Chair in Cell Biology. Y.K. is an incumbent of The Jack H. Skirball Chair for Applied Neurobiology. The IMB is a Special Research Centre of the Australian Research Council.

REFERENCES

1. **Apolloni, A., I. A. Prior, M. Lindsay, R. G. Parton, and J. F. Hancock.** 2000. H-ras but not K-ras traffics to the plasma membrane through the exocytic pathway. Mol. Cell. Biol. **20:**2475–2487.
2. **Axelrod, D., D. E. Koppel, J. Schlessinger, E. Elson, and W. W. Webb.** 1976. Mobility measurement by analysis of fluorescence photobleaching recovery kinetics. Biophys. J. **16:**1055–1069.
3. **Baker, T. L., H. Zheng, J. Walker, J. L. Coloff, and J. E. Buss.** 2003. Distinct rates of palmitate turnover on membrane-bound cellular and oncogenic H-ras. J. Biol. Chem. **278:**19292–19300.
4. **Besag, J. E.** 1977. Contribution to the discussion of Dr. Ripley's paper. J. R. Statist. Soc. B. **39:**193–195.
5. **Bivona, T. G., I. Perez De Castro, I. M. Ahearn, T. M. Grana, V. K. Chiu, P. J. Lockyer, P. J. Cullen, A. Pellicer, A. D. Cox, and M. R. Philips.** 2003. Phospholipase Cgamma activates Ras on the Golgi apparatus apparatus by means of RasGRP1. Nature **424:**694–698.
6. **Bivona, T. G., and M. R. Philips.** 2003. Ras pathway signaling on endomembranes. Curr. Opin. Cell Biol. **15:**136–142.
7. **Chiu, V. K., T. Bivona, A. Hach, J. B. Sajous, J. Silletti, H. Wiener, R. L. Johnson II, A. D. Cox, and M. R. Philips.** 2002. Ras signalling on the endoplasmic reticulum and the Golgi apparatus. Nat. Cell Biol. **4:**343–350.
8. **Choy, E., V. K. Chiu, J. Silletti, M. Feoktistov, T. Morimoto, D. Michaelson, I. E. Ivanov, and M. R. Philips.** 1999. Endomembrane trafficking of ras: the CAAX motif targets proteins to the ER and Golgi apparatus. Cell **98:**69–80.
9. **Coleman, R. A., P. Rao, R. J. Fogelsong, and E. S. Bardes.** 1992. 2-Bromopalmitoyl-CoA and 2-bromopalmitate: promiscuous inhibitors of membrane-bound enzymes. Biochim. Biophys. Acta **1125:**203–209.
10. **Diggle, P. J., J. Mateu, and H. E. Clough.** 2000. A comparison between parametric and non-parametric approaches to the analysis of replicated spatial point patterns. Adv. Appl. Probab. **32:**331–343.
11. **Dunphy, J. T., W. K. Greentree, and M. E. Linder.** 2001. Enrichment of G-protein palmitoyltransferase activity in low density membranes: in vitro reconstitution of Galphai to these domains requires palmitoyltransferase activity. J. Biol. Chem. **276:**43300–43304.
12. **Ehrlich, M., A. Shmuely, and Y. I. Henis.** 2001. A single internalization signal from the di-leucine family is critical for constitutive endocytosis of the type II TGF-beta receptor. J. Cell Sci. **114:**1777–1786.

13. **Elson, E. L., and J. A. Reidler.** 1979. Analysis of cell surface interactions by measurements of lateral mobility. J. Supramol. Struct. **12:**481–489.
14. **Fukata, M., Y. Fukata, H. Adesnik, R. A. Nicoll, and D. S. Bredt.** 2004. Identification of PSD-95 palmitoylating enzymes. Neuron **44:**987–996.
15. **Gorfe, A. A., R. Pellarin, and A. Caflisch.** 2004. Membrane localization and flexibility of a lipidated ras peptide studied by molecular dynamics simulations. J. Am. Chem. Soc. **126:**15277–15286.
16. **Hancock, J. F.** 2003. Ras proteins: different signals from different locations. Nat. Rev. Mol. Cell Biol. **4:**373–384.
17. **Hancock, J. F., K. Cadwallader, and C. J. Marshall.** 1991. Methylation and proteolysis are essential for efficient membrane binding of prenylated p21K-ras(B). EMBO J. **10:**641–646.
18. **Hancock, J. F., K. Cadwallader, H. Paterson, and C. J. Marshall.** 1991. A CAAX or a CAAL motif and a second signal are sufficient for plasma membrane targeting of ras proteins. EMBO J. **10:**4033–4039.
19. **Hancock, J. F., A. I. Magee, J. E. Childs, and C. J. Marshall.** 1989. All ras proteins are polyisoprenylated but only some are palmitoylated. Cell **57:** 1167–1177.
20. **Hancock, J. F., and R. G. Parton.** 2005. Ras plasma membrane signalling platforms. Biochem. J. **389:**1–11.
21. **Hancock, J. F., H. Paterson, and C. J. Marshall.** 1990. A polybasic domain or palmitoylation is required in addition to the CAAX motif to localize p21ras to the plasma membrane. Cell **63:**133–139.
22. **Hua, X., J. Sakai, M. S. Brown, and J. L. Goldstein.** 1996. Regulated cleavage of sterol regulatory element binding proteins requires sequences on both sides of the endoplasmic reticulum membrane. J. Biol. Chem. **271:** 10379–10384.
23. **Huang, K., A. Yanai, R. Kang, P. Arstikaitis, R. R. Singaraja, M. Metzler, A. Mullard, B. Haigh, C. Gauthier-Campbell, C. A. Gutekunst, M. R. Hayden, and A. El-Husseini.** 2004. Huntingtin-interacting protein HIP14 is a palmitoyl transferase involved in palmitoylation and trafficking of multiple neuronal proteins. Neuron **44:**977–986.
24. **Huster, D., A. Vogel, C. Katzka, H. A. Scheidt, H. Binder, S. Dante, T. Gutberlet, O. Zschornig, H. Waldmann, and K. Arnold.** 2003. Membrane insertion of a lipidated ras peptide studied by FTIR, solid-state NMR, and neutron diffraction spectroscopy. J. Am. Chem. Soc. **125:**4070–4079.
25. **Illenberger, D., C. Walliser, J. Strobel, O. Gutman, H. Niv, V. Gaidzik, Y. Kloog, P. Gierschik, and Y. I. Henis.** 2003. Rac2 regulation of phospholipase C-beta 2 activity and mode of membrane interactions in intact cells. J. Biol. Chem. **278:**8645–8652.
26. **Janosch, S., C. Nicolini, B. Ludolph, C. Peters, M. Volkert, T. L. Hazlet, E. Gratton, H. Waldmann, and R. Winter.** 2004. Partitioning of dual-lipidated peptides into membrane microdomains: lipid sorting vs peptide aggregation. J. Am. Chem. Soc. **126:**7496–7503.
27. **Jiang, X., and A. Sorkin.** 2002. Coordinated traffic of Grb2 and Ras during epidermal growth factor receptor endocytosis visualized in living cells. Mol. Biol. Cell **13:**1522–1535.
28. **Kanaani, J., D. el-Husseini Ael, A. Aguilera-Moreno, J. M. Diacovo, D. S. Bredt, and S. Baekkeskov.** 2002. A combination of three distinct trafficking signals mediates axonal targeting and presynaptic clustering of GAD65. J. Cell Biol. **158:**1229–1238.
29. **Linder, M. E., and R. J. Deschenes.** 2004. Model organisms lead the way to protein palmitoyltransferases. J. Cell Sci. **117:**521–526.
30. **Lobo, S., W. K. Greentree, M. E. Linder, and R. J. Deschenes.** 2002. Identification of a Ras palmitoyltransferase in Saccharomyces cerevisiae. J. Biol. Chem. **277:**41268–41273.
31. **Lu, J. Y., and S. L. Hofmann.** 1995. Depalmitoylation of CAAX motif proteins. Protein structural determinants of palmitate turnover rate. J. Biol. Chem. **270:**7251–7256.
32. **Magee, A. I., L. Gutierrez, I. A. McKay, C. J. Marshall, and A. Hall.** 1987. Dynamic fatty acylation of p21N-ras. EMBO J. **6:**3353–3357.
33. **Magee, A. I., and M. C. Seabra.** 2005. Fatty acylation and prenylation of proteins: what's hot in fat. Curr. Opin. Cell Biol. **17:**190–196.
34. **Niv, H., O. Gutman, Y. I. Henis, and Y. Kloog.** 1999. Membrane interactions of a constitutively active GFP-Ki-ras 4B and their role in signaling. Evidence from lateral mobility studies. J. Biol. Chem. **274:**1606–1613.
35. **Niv, H., O. Gutman, Y. Kloog, and Y. I. Henis.** 2002. Activated K-ras and H-ras display different interactions with saturable nonraft sites at the surface of live cells. J. Cell Biol. **157:**865–872.
36. **Parton, R. G., and J. F. Hancock.** 2001. Caveolin and Ras function. Methods Enzymol. **333:**172–183.
37. **Parton, R. G., and J. F. Hancock.** 2004. Lipid rafts and plasma membrane microorganization: insights from Ras. Trends Cell Biol. **14:**141–147.
38. **Perez de Castro, I., T. G. Bivona, M. R. Philips, and A. Pellicer.** 2004. Ras activation in Jurkat T cells following low-grade stimulation of the T-cell receptor is specific to N-ras and occurs only on the Golgi apparatus apparatus. Mol. Cell. Biol. **24:**3485–3496.
39. **Petersen, N. O., and E. L. Elson.** 1986. Measurements of diffusion and chemical kinetics by fluorescence photobleaching recovery and fluorescence correlation spectroscopy. Methods Enzymol. **130:**454–484.
40. **Plowman, S., C. Muncke, R. G. Parton, and J. F. Hancock.** H-ras, K-ras and inner plasma membrane raft proteins operate in nanoclusters with differential dependence on the actin cytoskeleton. Submitted for publication.
41. **Prior, I. A., A. Harding, J. Yan, J. Sluimer, R. G. Parton, and J. F. Hancock.** 2001. GTP-dependent segregation of H-ras from lipid rafts is required for biological activity. Nat. Cell Biol. **3:**368–375.
42. **Prior, I. A., C. Muncke, R. G. Parton, and J. F. Hancock.** 2003. Direct visualization of Ras proteins in spatially distinct cell surface microdomains. J. Cell Biol. **160:**165–170.
43. **Prior, I. A., R. G. Parton, and J. F. Hancock.** 2003. Observing cell surface signaling domains using electron microscopy. Sci. STKE **177:**pl9.
44. **Resh, M. D.** 1996. Regulation of cellular signalling by fatty acid acylation and prenylation of signal transduction proteins. Cell Signal. **8:**403–412.
45. **Ripley, B. D.** 1977. Modelling spatial patterns. J. R. Statist. Soc. B. **39:**172–192.
46. **Rizzo, M. A., C. A. Kraft, S. C. Watkins, E. S. Levitan, and G. Romero.** 2001. Agonist-dependent traffic of raft-associated Ras and Raf-1 is required for activation of the mitogen-activated protein kinase cascade. J. Biol. Chem. **276:**34928–34933.
47. **Rocks, O., A. Peyker, M. Kahms, P. J. Verveer, C. Koerner, M. Lumbierres, J. Kuhlmann, H. Waldmann, A. Wittinghofer, and P. I. Bastiaens.** 2005. An acylation cycle regulates localization and activity of palmitoylated Ras isoforms. Science **307:**1746–1752.
48. **Rotblat, B., I. A. Prior, C. Muncke, R. G. Parton, Y. Kloog, Y. I. Henis, and J. F. Hancock.** 2004. Three separable domains regulate GTP-dependent association of H-ras with the plasma membrane. Mol. Cell. Biol. **24:**6799–6810.
49. **Roy, S., A. Lane, J. Yan, R. McPherson, and J. F. Hancock.** 1997. Activity of plasma membrane-recruited Raf-1 is regulated by Ras via the Raf zinc finger. J. Biol. Chem. **272:**20139–20145.
50. **Roy, S., R. Luetterforst, A. Harding, A. Apolloni, M. Etheridge, E. Stang, B. Rolls, J. F. Hancock, and R. G. Parton.** 1999. Dominant-negative caveolin inhibits H-ras function by disrupting cholesterol-rich plasma membrane domains. Nat. Cell Biol. **1:**98–105.
51. **Roy, S., B. Wyse, and J. F. Hancock.** 2002. H-ras signaling and K-ras signaling are differentially dependent on endocytosis. Mol. Cell. Biol. **22:**5128–5140.
52. **Schroeder, H., R. Leventis, S. Rex, M. Schelhaas, E. Nagele, H. Waldmann, and J. R. Silvius.** 1997. S-acylation and plasma membrane targeting of the farnesylated carboxyl-terminal peptide of N-ras in mammalian fibroblasts. Biochemistry **36:**13102–13109.
53. **Shvartsman, D. E., M. Kotler, R. D. Tall, M. G. Roth, and Y. I. Henis.** 2003. Differently anchored influenza hemagglutinin mutants display distinct interaction dynamics with mutual rafts. J. Cell Biol. **163:**879–888.
54. **van't Hof, W., and M. D. Resh.** 1997. Rapid plasma membrane anchoring of newly synthesized p59fyn: selective requirement for NH2-terminal myristoylation and palmitoylation at cysteine-3. J. Cell Biol. **136:**1023–1035.
55. **Verkruyse, L. A., and S. L. Hofmann.** 1996. Lysosomal targeting of palmitoyl-protein thioesterase. J. Biol. Chem. **271:**15831–15836.
56. **Webb, Y., L. Hermida-Matsumoto, and M. D. Resh.** 2000. Inhibition of protein palmitoylation, raft localization, and T cell signaling by 2-bromopalmitate and polyunsaturated fatty acids. J. Biol. Chem. **275:**261–270.
57. **Zhao, L., S. Lobo, X. Dong, A. D. Ault, and R. J. Deschenes.** 2002. Erf4p and Erf2p form an endoplasmic reticulum-associated complex involved in the plasma membrane localization of yeast Ras proteins. J. Biol. Chem. **277:** 49352–49359.